frontiers | Frontiers in Chemistry

MINI REVIEW
published: 07 April 2022
doi: 10.3389/fchem.2022.870564

Recent Advances in Antimony Sulfide-Based Nanomaterials for High-Performance Sodium-Ion Batteries: A Mini Review

Guangxin Wang[1†], Mingyi Guo[1†], Yunchao Zhao[1,2], Yibo Zhao[1], Kun Tang[1], Zhijun Chen[3], Heinz-Rolf Stock[1] and Yong Liu[1,2*]*

[1]*Research Center for High Purity Materials, Henan University of Science and Technology, Luoyang, China,* [2]*Provincial and Ministerial Co-Construction of Collaborative Innovation Center for Non-Ferrous Metal New Materials and Advanced Processing Technology, Henan Key Laboratory of Non-Ferrous Materials Science and Processing Technology, School of Materials Science and Engineering, Henan University of Science and Technology, Luoyang, China,* [3]*Luoyang Bearing Research Institute Co., Ltd, Luoyang, China*

Recently, sodium-ion batteries (SIBs) have attracted extensive attention as potential alternatives to lithium-ion batteries (LIBs) due to the abundance, even distribution, low cost, and environmentally friendly nature of sodium. However, sodium ions are larger than lithium ions so that the anode materials of LIBs are not suitable for SIBs. Therefore, many negative electrode materials have been investigated. Among them, Sb_2S_3-based nanomaterials have gradually become a research focus due to their high theoretical specific capacity, good thermal stability, simple preparation, and low price. In this review, the research progress of Sb_2S_3-based nanomaterials in the SIB field in recent years is summarized, including Sb_2S_3, Sb_2S_3/carbon composites, Sb_2S_3/graphene composites, and Sb_2S_3/M_xS_y composites. Furthermore, the challenges and prospects for the development of Sb_2S_3-based nanomaterials are also put forward. We hope this review will contribute to the design and manufacture of high-performance SIBs and promote its practical application.

Keywords: sodium-ion batteries, electrochemical performance, Sb_2S_3-based nanomaterials, anode materials, composites

OPEN ACCESS

Edited by:
Jinlin Lu,
Guangzhou Maritime College, China

Reviewed by:
Zhenyu Xing,
South China Normal University, China
Hongshuai Hou,
Central South University, China

****Correspondence:***
Mingyi Guo
gmy19910513@163.com
Yong Liu
liuyong209@haust.edu.cn

[†]These authors have contributed equally to this work

Specialty section:
This article was submitted to Nanoscience, a section of the journal Frontiers in Chemistry

Received: *07 February 2022*
Accepted: *24 February 2022*
Published: *07 April 2022*

Citation:
Wang G, Guo M, Zhao Y, Zhao Y, Tang K, Chen Z, Stock H-R and Liu Y (2022) Recent Advances in Antimony Sulfide-Based Nanomaterials for High-Performance Sodium-Ion Batteries: A Mini Review. Front. Chem. 10:870564. doi: 10.3389/fchem.2022.870564

INTRODUCTION

Recently, lithium-ion batteries (LIBs) have developed rapidly and are extensively used in electronic devices such as notebook computers, electric vehicles, and mobile phones (Qin et al., 2017; Chong et al., 2018; Schmuch et al., 2018; Pang et al., 2019; Yuan et al., 2019; Wang et al., 2020; Tao et al., 2022). Nevertheless, the distribution of lithium on earth is uneven, and its reserves are limited. In addition, there are still some problems that need to be solved for LIBs, such as poor low-temperature performance, safety problems, and high cost (Liu G. et al., 2018; Xing et al., 2020; Sui D. et al., 2021; Wang et al., 2021c; Shi et al., 2021). As a potential substitute for LIBs in energy storage devices, SIBs have attracted extensive attention because sodium is much cheaper than lithium, environmentally friendly, and SIBs show the same energy storage mechanism as LIBs (Wang et al., 2018; Cao et al., 2020; Sui et al., 2020). However, the ionic radius of sodium ion (Na^+: 102 p.m.) is larger than that of lithium ion (Li^+: 76 p.m.), which will lead to difficulties in the sodiation/desodiation process combined with a greater volume change. Consequently, electrode materials matched with LIBs are

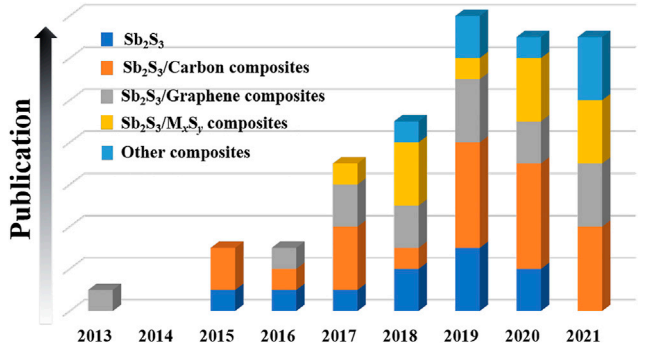

FIGURE 1 | Bar chart of Sb_2S_3-based nanomaterials as anodes for SIBs in recent years.

not suitable for SIBs (Zhao and Arumugam, 2015; Wang et al., 2017; Liu Q. et al., 2019; Liu Y. et al., 2019; Hao et al., 2019; Sui et al., 2020). Therefore, it is critical to investigate SIB electrode materials with high reversible capacity and excellent cycle stability.

As an important type of electrode material for SIBs, anode materials have been widely studied (Tao et al., 2021). Until now, considerable achievements have been made in the research of SIB anode materials, such as layered transition metal oxides (Xiong et al., 2011; Ma et al., 2020; Li Y. et al., 2020), polyanionic compounds (Li et al., 2015; Yu et al., 2018; Guo et al., 2020; Sui Y. et al., 2021), metal sulfide composites (Cui et al., 2018; Zhao et al., 2020), or alloy composites (Liu et al., 2016; Tao et al., 2021). Metal sulfide anodes have a higher sodium storage capacity, and generally have lower redox potential, better electrochemical reversibility, and longer cycle life than metal oxides in charge/discharge reaction (Xie et al., 2018; Liu G. et al., 2019; Xu et al., 2019; Yao et al., 2019; Shan et al., 2020). Among them, Sb_2S_3 has a high theoretical capacity of 946 mA h g^{-1}, and it is cheap and harmless to the environment (Zhu et al., 2015; Xie F. et al., 2019). Moreover, by combining the conversion reaction (**Eq. 1**) and alloying reaction (**Eq. 2**) between Na and S, Sb_2S_3 can produce a high-capacity anode and effectively play the role of S–Na and Sb–Na nanocomposites in SIBs (Yu et al., 2013; Liu et al., 2017). The following is the generally proposed electrochemical reaction mechanism between Sb_2S_3 and Na^+ (Liu et al., 2017; Xie F. et al., 2019):

$$\text{Conversion reaction}: Sb_2S_3 + 6Na^+ + 6e^- \rightarrow 2Sb + 3Na_2S. \quad (1)$$

$$\text{Alloying reaction}: 2Sb + 6Na^+ + 6e^- \rightarrow 2Na_3S. \quad (2)$$

Sb_2S_3-based anode materials, such as multi-shell hollow Sb_2S_3 (Xie F. et al., 2019), Sb_2S_3/graphene composites (Li C.-Y. et al., 2017; Zhao et al., 2021), Sb_2S_3@FeS_2/N-graphene (SFS/C) (Cao et al., 2020), and L-Sb_2S_3/Ti_3C_2 composites (He et al., 2021), have been reported in the application field of SIBs. For instance, Xiong et al. reported about Sb_2S_3 with nanostructure on S-doped graphene sheets for high-performance anode materials of SIBs (Xiong et al., 2016). Based on the interaction of heterogeneous interfaces between different components of metal sulfide, Cao et al. reported Sb_2S_3@FeS_2 with heteroatom-doped graphene as a superior SIB anode material (Cao et al., 2020). Xu et al. (2019) reviewed updated research on multiple phase transformation mechanisms and strategies to improve the performance of Sb- and Bi-based chalcogenides for SIBs. Liu et al. reviewed recent studies on Sb-based electrode materials for applications, storage mechanisms, and synthesis strategies in SIBs, LIBs, and LMBs (liquid metal batteries) (Liu Z. et al., 2018). However, so far as we know, critical reviews that focus on Sb_2S_3-based electrode nanomaterials specifically for SIBs have rarely been reported.

Herein, the research achievements and progresses of Sb_2S_3-based nanomaterials for SIBs in recent years are summarized (see **Figure 1**). In addition, some rational suggestions on the research and design of Sb_2S_3-based nanomaterials for SIBs in the future are also presented. Finally, we hope that this review can attract more attention and promote the practical applications of Sb_2S_3-based nanomaterials in the SIB field.

RESEARCH PROGRESS OF SB_2S_3-BASED NANOMATERIALS IN HIGH-PERFORMANCE SIBS

Sb_2S_3 has advantages of low price, simple preparation, and good thermal stability (Xie F. et al., 2019; Cao et al., 2020). It is promising to be used as anode materials for high-capacity SIBs. A variety of Sb_2S_3-based anode materials have been reported. These are listed in **Table 1**.

Sb_2S_3

To obtain Sb_2S_3 anodes with high energy density and capacity in SIBs, researchers prepared Sb_2S_3 with different morphologies, such as amorphous Sb_2S_3 (Hwang et al., 2016), flower-like Sb_2S_3 (Zhu et al., 2015), multi-shell Sb_2S_3 (Xie F. et al., 2019), or Sb_2S_3 hollow microspheres (Xie et al., 2018).

For example, Hwang et al. (2016) synthesized aspherical, amorphous α-Sb_2S_3 *via* a facile polyol route at room temperature, which is different from the previous routes of forming crystalline Sb_2S_3 at high temperature (mainly, hydrothermal method) (Zhu et al., 2015). As shown in **Supplementary Figure S1A**, α-Sb_2S_3 nanoparticles were composed of spherical aggregates of sub-component nanoparticles with diameters of 150–300 nm. When investigated as SIB anodes, the α-Sb_2S_3 nanoparticle electrode displayed a charge capacity of 512 mA h g^{-1} after 100 cycles at a current density of 50 mA g^{-1}, and showed a better cycle performance and excellent rate performance, in contrast with the commercial crystal Sb_2S_3 electrode (**Supplementary Figure S1B**).

Moreover, two-dimensional (2D) nanomaterials with large surface area and ultrafine thickness have attracted more and more attention. For instance, Yao et al. (2019) designed 2D-Sb_2S_3 nanosheets by using a facile and scalable Li intercalation assisted stripping method. The 2D-Sb_2S_3 nanosheets (2D-SS) showed a good layered structure with a mean thickness of 3.8 nm (**Supplementary Figure S1C**). The large pore volume and

TABLE 1 | Electrochemical performances of Sb_2S_3-based nanomaterials as anodes for SIBs.

Materials	Initial Coulomb Efficiency [%]	Capacity [mAh g^{-1}/ Cycles]	Rate capability [mAh g^{-1}]	Ref
Sb_2S_3				
Sb_2S_3	72.4	195 (200) at 0.1 A g^{-1}	–	Fu et al. (2019)
Amorphous Sb_2S_3	65	512 (100) at 0.05 A g^{-1}	534 at 3 A g^{-1}	Hwang et al. (2016)
Sb_2S_3 micro tubes	37.1	201 (20) at 0.1 A g^{-1}	286 at 0.2 A g^{-1}	Jin Pan et al. (2017)
Colloidal Sb_2S_3	–	580 (100) at 0.3 A g^{-1}	620 at 1.2 A g^{-1}	Kravchyk et al. (2020)
Single crystal Sb_2S_3	50	579 (50) at 0.1 A g^{-1}	358 at 1 A g^{-1}	Pan et al. (2018a)
Sb_2S_3 hollow microspheres	62	384 (50) at 0.2 A g^{-1}	386 at 2 A g^{-1}, 314 at 3 A g^{-1}	Xie et al. (2018)
Multi-shell Sb_2S_3	55	909 (50) at 0.1 A g^{-1}	725 at 1 A g^{-1},604 at 2 A g^{-1}	Xie et al. (2019a)
2D-Sb_2S_3	-	500 (100) at 0.2 A g^{-1}	300 at 2 A g^{-1}	Yao et al. (2019)
Sb_2S_3	77.6	38.6 (200) at 0.1 A g^{-1}	109.5 at 1 A g^{-1}, 95.1 at 2 A g^{-1}	Zhao et al. (2020)
Flower-like Sb_2S_3	72.9	641.7 (100) at 0.2 A g^{-1}	597.9 at 1A g^{-1}, 554.6 at 2 A g^{-1}	Zhu et al. (2015)
Sb_2S_3/carbon composites				
Sb_2S_3@YP-43%	42.6	736.2 (100) at 0.23 A g^{-1}	476.5 (1,000) at 1.2 A g^{-1}	Chang et al. (2020b)
Sb_2S_3/P/C	79	611 (100) at 0.05 A g^{-1}	390 at 2 A g^{-1}	Choi et al. (2016)
Sb_2S_3/C	78	538 (100) at 0.2 A g^{-1}	579 at 0.5A g^{-1}, 557 at 1 A g^{-1}	Choi et al. (2017)
Sb_2S_3@C	38.2	267 (100) at 0.1 A g^{-1}	283 at 1 A g^{-1}	Dashairya et al. (2021)
Sb_2S_3/SCS	68.8	455.8 (100) at 0.1 A g^{-1}	392 (15) at 0.5 A g^{-1}, 263 (20) at 1 A g^{-1}	Deng et al. (2019)
Sb_2S_3@N-C	80	765 (10) at 0.1 A g^{-1}	625 (1,000) at 1 A g^{-1}	Dong et al. (2019)
Sb_2S_3@C rods	68.5	699.1 (100) at 0.1 A g^{-1}	578 at 1.5A g^{-1}, 429 at 3.2 A g^{-1}	Hongshuai Hou et al. (2015)
Sb_2S_3/C	–	545.6 (100) at 0.2 A g^{-1}	550.8 (70) at 0.2 A g^{-1}	Ge et al. (2018)
M-Sb_2S_3@DC	–	326 (100) at 0.5 A g^{-1}	451 at 1 A g^{-1},366 at 3 A g^{-1}	Ge et al. (2020)
Sb_2S_3/CM	64.7	426 (150) at 0.1 A g^{-1}	–	Jaramillo-Quintero et al. (2021)
Sb_2S_3/Sb-CM	67.1	608 (150) at 0.1 A g^{-1}	–	Jaramillo-Quintero et al. (2021)
Sb_2S_3/S-CM	66.9	675 (150) at 0.1 A g^{-1}	552 at 1 A g^{-1}, 481 at 2 A g^{-1}	Jaramillo-Quintero et al. (2021)
Sb_2S_3@CNTs	66.4	732 (110) at 0.05 A g^{-1}	668 at 1 A g^{-1}, 584 at 2 A g^{-1}	Jiang et al. (2021)
Sb_2S_3@MWCNTs	79.2	412.3 (50) at 0.05 A g^{-1}	368.8 at 0.5 A g^{-1}, 339.1 at 1 A g^{-1}	Li et al. (2017b)
Amorphous Sb_2S_3/CNT	77.8	704 (50) at 0.1 A g^{-1}	601 at 2 A g^{-1},474 at 3 A g^{-1}	Li et al. (2019)
Sb_2S_3/CFC	76	736 (650) at 0.5 A g^{-1}	649 (400) at 2 A g^{-1}, 585 (400) at 5 A g^{-1}	Liu et al. (2017)
CPC/Sb_2S_3	80	443 at 0.1 A g^{-1}	220 (200) at 1 A g^{-1}	Mullaivananathan and Kalaiselvi, (2019)
Sb_2S_3/CS	60	321 (200) at 0.2 A g^{-1}	221 at 5 A g^{-1}	Xie et al. (2019b)
Sb_2S_3@CNF	57.4	267.8 (100) at 0.1 A g^{-1}	221 at 1 A g^{-1},178 at 5 A g^{-1}	Zhai et al. (2020)
Sb_2S_3@NCFs	56.5	412 (50) at 0.05 A g^{-1}	291 at 1 A g^{-1}, 244 at 2 A g^{-1}	Zhang et al. (2021b)
SS/Sb@C-1	70.9	171 (200) at 0.1 A g^{-1}	253.2 at 1A g^{-1}, 202.8 at 2 A g^{-1}	Zhao et al. (2020)
SS/Sb@C-2	66.4	474.6 (200) at 0.1 A g^{-1}	367 (150) at 1 A g^{-1},311.1 (150) at 2 A g^{-1}	Zhao et al. (2020)
Sb_2S_3/graphite	84	733 at 0.1 A g^{-1}	656 (100) at 1 A g^{-1}, 495 (100) at 10 A g^{-1}	Zhao. and Manthiram, (2015)
Sb_2S_3/graphene composites				
SN-RGO/Sb_2S_3	57	507 (150) at 0.1 A g^{-1}	443.46 at 1 A g^{-1}, 364.89 at 2 A g^{-1}	Bag et al. (2019)
Sb_2S_3/RGO	55.9	262 (100) at 0.1 A g^{-1}	210 at 1 A g^{-1}	Dashairya et al. (2021)
Sb_2S_3/RGO	75.6	220 (50) at 0.05 A g^{-1}	–	Dashairya and Saha, (2020)
Sn@Sb_2S_3-RGO	69.8	597.6 (60) at 0.2 A g^{-1}	541 (70) at 0.5 A g^{-1}	Deng et al. (2018)
Sb_2S_3/RGO	66.4	555 (70) at 0.1 A g^{-1}	–	Fan and Xie, (2019)
Sb_2S_3/graphene	–	760 (100) at 0.05 A g^{-1}	420 (100) at 1.5 A g^{-1}	Li et al. (2017a)
Sb_2S_3/RGO	–	687.7 (80) at 0.05 A g^{-1}	495.1 (80) at 0.2 A g^{-1},414.8 (100) at 0.5 A g^{-1}	Pan et al. (2018b)
Sb_2S_3/RGO	52.6	652 (60) at 0.1 A g^{-1}	527 at 1 A g^{-1}, 381 at 2 A g^{-1}	Wen et al. (2019)
Sb_2S_3/RGO	85.7	581.2 (50) at 0.05 A g^{-1}	309.8 (10) at 2 A g^{-1}	Wu et al. (2017)
Sb_2S_3/SGS	–	524.4 (900) at 2 A g^{-1}	591.6 at 5 A g^{-1}	Xiong et al. (2016)
RGO/Sb_2S_3	69.2	670 (50) at 0.05 A g^{-1}	611 (5) at 1.5 A g^{-1}, 520 (5) at 3 A g^{-1}	Yu et al. (2013)
Sb_2S_3@N-C/RGO	57.6	368 (200) at 0.2 A g^{-1}	338 at 1 A g^{-1}, 253 at 5 A g^{-1}	Zhan et al. (2021)
Sb_2S_3–graphene	55.9	881.2 (50) at 0.1 A g^{-1}	536.4 at 1 A g^{-1}	Zhao et al. (2021)
S-RGO/Sb_2S_3	63.9	509 (200) at 0.1 A g^{-1}	239 (2000) at 5 A g^{-1}	Zhou et al. (2020b)
Sb2S3/MxSy composites				
Sb_2S_3@FeS_2/N-graphene (SFS/C)	82.4	725.4 at 0.1 A g^{-1}	645.6 at 1A g^{-1}, 564.3 at 5 A g^{-1}	Cao et al. (2020)
Sb_2S_3-SnS_2	77.9	616 (50) at 0.5 A g^{-1}	510 at 10 A g^{-1}	Fang et al. (2019)
In_2S_3-Sb_2S_3@MCNTs	–	454 (40) at 0.2 A g^{-1}	402 at 1.6 A g^{-1},355 at 3.2 A g^{-1}	Huang et al. (2018)
Sb_2S_3/MoS_2 NWs	82.9	800 at 0.1 A g^{-1}	570 at 3.2 A g^{-1}	Li P. et al. (2020)
Sb_2S_3-Bi_2S_3@C@RGO	68.1	600.7 (150) at 1 A g^{-1}	514.5 at 5 A g^{-1}, 485.8 at 8 A g^{-1}	Li et al. (2021)
Sb_2S_3@SnS@C	79	516 (100) at 0.1 A g^{-1}	442 (200) at 1 A g^{-1}, 200 (1,300) at 5 A g^{-1}	Lin et al. (2021)

(Continued on following page)

TABLE 1 | (*Continued*) Electrochemical performances of Sb_2S_3-based nanomaterials as anodes for SIBs.

Materials	Initial Coulomb Efficiency [%]	Capacity [mAh g^{-1}/ Cycles]	Rate capability [mAh g^{-1}]	Ref
ZnS-Sb_2S_3@C	61.4	630 (120) at 0.1 A g^{-1}	390.6 at 0.8 A g^{-1}	Dong et al. (2017)
SnS_2/Sb_2S_3@RGO	82.3	642 (100) at 0.2 A g^{-1}	593 at 2 A g^{-1}, 567 at 4 A g^{-1}	Wang et al. (2018)
Sb_2S_3/MoS_2@C (SMS@C)	79.5	623.2 at 0.1 A g^{-1}	465.6 (100) at 1 A g^{-1}, 411.5 (650) at 5 A g^{-1}	Wang et al. (2021a)
Sb_2S_3/MoS_2	75.9	568.4 at 0.1 A g^{-1}	423.2 (100) at 1 A g^{-1}	Wang et al. (2021a)
Sb_2S_3/MoS_2	48.5	561 (100) at 0.1 A g^{-1}	628 at 1A g^{-1}, 507 at 2 A g^{-1}	Zhang et al. (2018)
α-Sb_2S_3@$CuSbS_2$	82.2	506.7 (50) at 0.05 A g^{-1}	293 at 3 A g^{-1}	Zhou et al. (2020a)
Other composites				
Sb_2S_3@SnO_2	54.2	582.9 (100) at 0.05 A g^{-1}	441.6 at 1A g^{-1}, 237.1 at 5 A g^{-1}	Chang et al. (2020a)
L-Sb_2S_3/Ti_3C_2	65.7	445.5 (100) at 0.1 A g^{-1}	339.5 at 2 A g^{-1}	He et al. (2021)
Sb_2S_3@$Ti_3C_2T_x$		329 (100) at 0.1 A g^{-1}	118 (500) at 2 A g^{-1}	Ren et al. (2021)
Sb_2S_3@PPy	63.7	881 (50) at 0.1 A g^{-1}	390 (400) at 2 A g^{-1}	Shi et al. (2019)
Sb_2S_3/MMCN@PPy	–	446 (50) at 0.1 A g^{-1}	269 (300) at 1 A g^{-1}	Yin et al. (2019)
Sb_2S_3@m-$Ti_3C_2T_x$	51	156 (100) at 0.1 A g^{-1}	72 (1000) at 2 A g^{-1}	Zhang et al. (2021a)
Sb_2S_3/PPy	70	427 (50) at 0.1 A g^{-1}	236 (50) at 0.5 A g^{-1}	Zheng et al. (2018)

Notes: 2D-Sb_2S_3 = two-dimensional Sb_2S_3; Sb_2S_3@YP-43% = 43% contents Sb_2S_3 mixed with YP80F active carbon (YP); Sb_2S_3/SCS, stibnite/sulfur-doped carbon sheet; M-Sb_2S_3@DC, metal-sulfides with double carbon; CM, carbon matrix; CNTs, carbon nanotubes; MWCNTs, multiwalled carbon nanotubes; CFC, carbon fiber cloth; CPC, coir pith derived carbon; Sb_2S_3/CS, Sb_2S_3 embedded in carbon–silicon oxide nanofibers; CNF, multichannel N-doped carbon nanofiber; NCFs = N-doped 3D carbon nanofibers; RGO, reduced graphene oxide; Sb_2S_3/SGS, Sb_2S_3/sulfur-doped graphene sheets; SN-RGO/Sb_2S_3 = sulfur, nitrogen dual doped RGO/Sb_2S_3; Sb_2S_3@N-C/RGO, Sb_2S_3/nitrogen-doped carbon/RGO; S-RGO/Sb_2S_3 = sulfur-doped RGO/Sb_2S_3; MCNTs, multiwalled carbon nanotubes; Sb_2S_3/MoS_2 NWs, Sb_2S_3/MoS_2 core-shell nanowires; PPy, polypyrrole.

large surface area of 2D-SS nanosheets are beneficial to the electrolyte penetration and the volume change during cycles. Therefore, 2D-SS nanosheet anodes showed remarkable rate capability and stable cycle performance in both SIBs and LIBs. When used in SIBs (**Supplementary Figure S1D**), the 2D-SS anode displayed a superior capacity of ~500 mA h g^{-1} after 100 cycles at 200 mA g^{-1} current rate.

Recently, Sb_2S_3 materials with three-dimensional (3D) hierarchical architecture were designed and synthesized to expand the contact surface area of the electrode and electrolyte and adapt it to volume expansion (Jin Pan et al., 2017; Xie et al., 2018; Xie F. et al., 2019). Xie et al. (2018) used $SbCl_3$ and $_L$-cysteine as raw materials and successfully synthesized Sb_2S_3 hollow microspheres by a hydrothermal method. The SEM image and cycling performance of Sb_2S_3 hollow microspheres are shown in **Supplementary Figures S1E,F**. However, large internal voids in hollow structures can greatly reduce bulk energy density. In order to obtain a high volumetric energy density and maintain a high gravimetric energy density, Xie F. et al. (2019) synthesized multi-shell hollow Sb_2S_3 structures using the metal-organic framework templates (MOFs) (**Supplementary Figure S1G**). Used as an anode in SIBs (**Supplementary Figure S1H**), the multi-shell Sb_2S_3 exhibited reversible capacities of 909, 806, 725, and 604 mA h g^{-1} at various currents of 100, 400, 1,000, and 2,000 mA g^{-1}, respectively, higher than the single-shell Sb_2S_3 structure.

Sb_2S_3/Carbon Composites

Carbon materials have received considerable attention because of their superior characteristics, such as large specific surface area, high conductivity, excellent flexibility, and chemical stability (Tao et al., 2021). During the use of SIBs, Sb_2S_3 will undergo transformation and alloying reaction, which results in excessive volume expansion/contraction of the material, and hinders the application of Sb_2S_3 energy storage effect. Therefore, Sb_2S_3 is usually combined with carbon materials to inhibit the volume change, such as Sb_2S_3/carbon-rods (Hongshuai Hou et al., 2015), Sb_2S_3/carbon-nanotubes (Li J. et al., 2017; Li et al., 2019), Sb_2S_3/carbon-nanofiber (Zhai et al., 2020; Zhang Q. et al., 2021), or Sb_2S_3/heteroatom-doped carbon (Dong et al., 2019; Jaramillo-Quintero et al., 2021).

For instance, Hongshuai Hou et al. (2015) designed one-dimensional (1D) Sb_2S_3@C rods as a distinctive anode material to improve the electrochemical performance of SIBs *via* a solvothermal method (**Supplementary Figure S2A**). The Sb_2S_3@C rod electrode could deliver 699.1 mA h g^{-1} at a current rate of 100 mA g^{-1} after 100 cycles (**Supplementary Figure S2B**). Liu et al. (2017) reported a hydrothermal method for preparing Sb_2S_3 micro-nanospheres loaded on carbon fiber cloth (CFC). The obtained composite materials were denoted as SS/CFC. The flexible carbon fiber cloth was completely covered by spherical Sb_2S_3 in **Supplementary Figure S2C**, which could greatly accommodate the volume change (Guo et al., 2019). When used as electrodes for SIBs (**Supplementary Figure S2D**), SS/CFC electrodes exhibited an excellent initial discharge capacity of 1,048 mA h g^{-1} at 0.5 A g^{-1}, and displayed a reversible capacity of 736 mA h g^{-1} after 650 cycles in the voltage range of 0.01–2.00 V. After two initial cycles, the corresponding Coulombic efficiency of SS/CFC rapidly increased to ~100%.

To boost the storage performance of SIBs, Sb_2S_3 can be combined with carbon doped with heteroatoms (e.g., N, S, P, and Sb), thus improving the conductivity, the storage regions, and the active sites (Choi et al., 2016; Dong et al., 2019; Zhai et al., 2020; Jaramillo-Quintero et al., 2021). For instance, Zhao et al. (2020) utilized the oxygen-function group of phenolic resin and

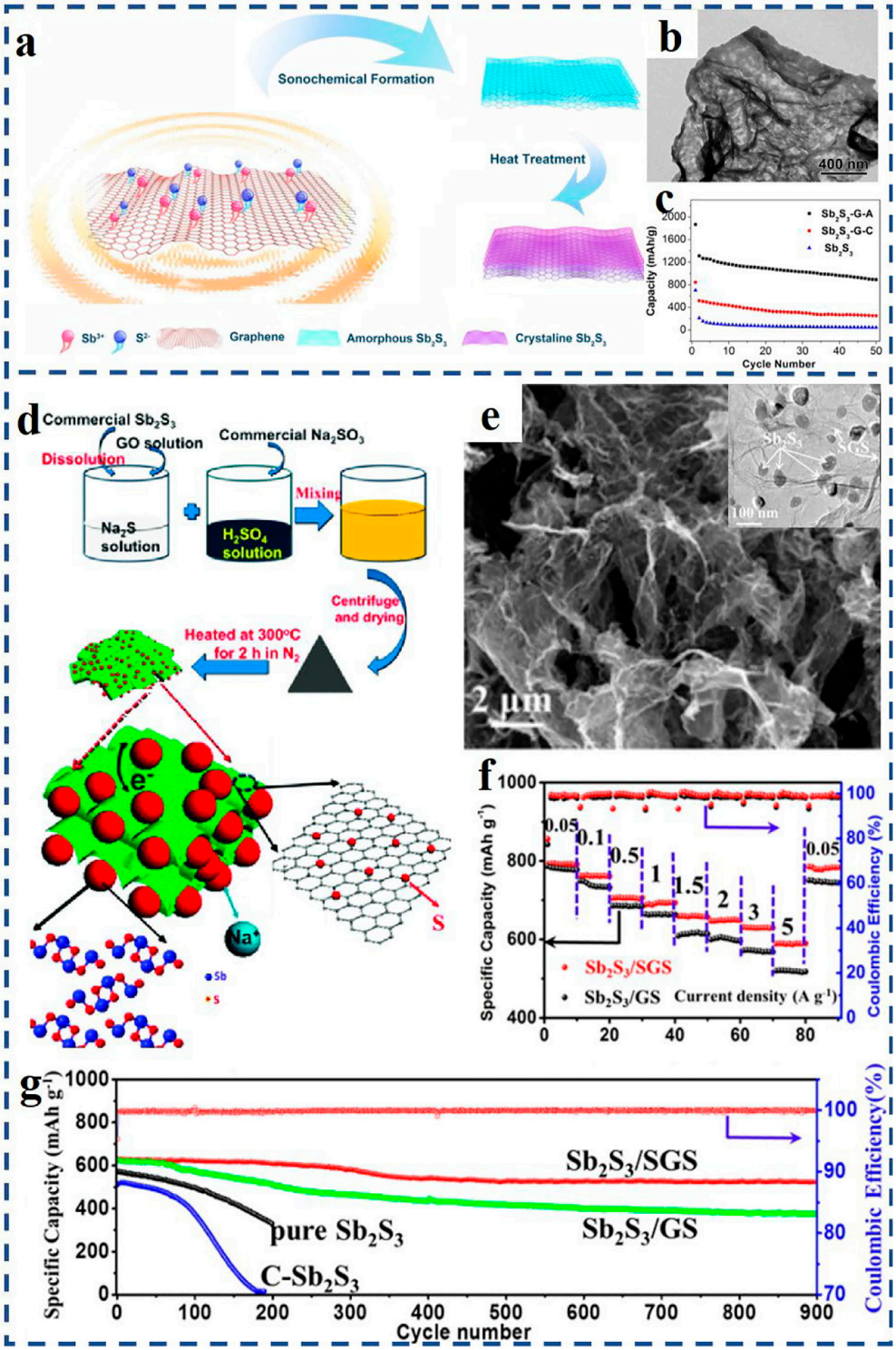

FIGURE 2 | (A) Schematic illustration of the preparation process of the amorphous and crystalline Sb_2S_3/graphene composites; **(B)** TEM image of the amorphous Sb_2S_3–graphene composites; **(C)** cycle performances of the pristine Sb_2S_3 and amorphous and crystalline Sb_2S_3–graphene electrodes (denoted as Sb_2S_3-G-A and Sb_2S_3-G-C); **(D)** formation process of the Sb_2S_3/S-doped graphene nanocomposite (Sb_2S_3/SGS); **(E)** SEM and TEM images of the Sb_2S_3/SGS nanocomposite; **(F)** rate performances of the Sb_2S_3/SGS electrode and Sb_2S_3–graphene electrode (Sb_2S_3/GS) under different current density; **(G)** cycle performances of three experimental electrodes at 2 A g^{-1}. **(A–C)** Reproduced with permission from Zhao et al. (2021). Copyright 2020, Elsevier. **(D–G)** Reproduced with permission from Xiong et al. (2016), Copyright 2016, American Chemical Society.

constructed Sb_2S_3 with hierarchical interfaces (antimony and sulfur-doped carbon) (**Supplementary Figure S2E**). The final obtained composites were denoted as SS/Sb@C. When evaluated as electrode materials for SIBs (**Supplementary Figure S2F**), SS/Sb@C delivered a reversible capacity of 474.6 mA h g^{-1} and a capacity retention rate of 97.1% after 200 cycles at 0.1 A g^{-1}, showing better cyclic stability and superior rate capability than those of the Sb_2S_3 anodes without heteroatoms (38.6 mA h g^{-1}). This was due to the double control synergy of Sb-shell structure and S-doped carbon structure, which effectively expanded the polysulfide diffusion path, enhanced the reversibility of conversion reaction, and thus improved the Na-storage capacity of SIBs (Yu et al., 2020; Wang et al., 2021b). This kind of reasonable design was expected to bring bright prospects for the design of metal sulfides as advanced anodes of SIBs.

Sb_2S_3/Graphene Composites

Graphene has high specific surface area, which is convenient for constructing interconnected pore structures to form conductive networks. In addition, it can also provide a platform for the growth of active materials (Lv et al., 2016; Sui et al., 2020; Wang X. et al., 2021; Liu et al., 2021). The combination of Sb_2S_3 with graphene can provide excellent Na^+ energy storage properties. Therefore, many composites have been designed in recent years, such as Sb_2S_3/RGO (RGO = reduced graphene oxide) (Yu et al., 2013; Wen et al., 2019), Sn@Sb_2S_3-RGO (tin assisted Sb_2S_3 decorated on RGO) (Deng et al., 2018), S-RGO/Sb_2S_3 (sulfur-doped RGO-based composite with Sb_2S_3) (Zhou X. et al., 2020), and Sb_2S_3/N-C/RGO (Sb_2S_3@nitrogen-doped carbon decorated on RGO) (Zhan et al., 2021), to improve the storage properties of SIBs.

For example, Yu et al. (2013) received a uniform coating of Sb_2S_3 on RGO (RGO/Sb_2S_3) through a solution-based synthesis method and applied it as SIB anode materials. The RGO/Sb_2S_3 composite with a small particle size of 15–30 nm allows Na^+ to move in and out of the particles rapidly during charge and discharge process. In addition, the 2D-layered structure of graphene and Sb_2S_3 can form oriented layered composites with excellent properties. Compared with traditional synthesis techniques, the ultrasound sonochemical method can create particular reaction conditions, and make it possible to prepare nanostructured materials with special properties by acoustic cavitation effects. Zhao et al. (2021) synthesized a special amorphous nanostructure composite material of Sb_2S_3/graphene by an ultrasound sonochemical synthesis technique (**Figure 2A**). As can be seen from **Figure 2B**, Sb_2S_3 nanoparticles were tightly covered on the graphene nanosheets and evenly distributed on both sides. The Sb_2S_3/graphene nanocomposites with amorphous structure had good tolerance and adaptability to drastic volume changes. Compared to the crystalline counterpart (Li C.-Y. et al., 2017), the amorphous Sb_2S_3/graphene nanocomposite displayed a superior electrochemical property with a higher reversible capacity of 881.2 mA h g^{-1} at 0.1 A g^{-1} after 50 cycles (**Figure 2C**).

Furthermore, doping heteroatoms (e.g., N, P, S, Sn) on graphene-based materials by surface chemical modification can effectively improve the properties of SIBs (Xiong et al., 2016; Deng et al., 2018; Zhou X. et al., 2020; Zhan et al., 2021). For example, Xiong et al. (2016) obtained a unique Sb_2S_3/S-doped graphene anode material (denoted as Sb_2S_3/SGS) *via* firm chemical binding of nano-Sb_2S_3 structure on S-doped graphene nanosheets (SGS). Schematic illustration of the preparation process of the Sb_2S_3/SGS composite is displayed in **Figure 2D**. As shown in **Figure 2E**, Sb_2S_3 nanoparticles are wrapped by flexible SGS and exhibit a size of 30–80 nm. When tested at 0.05 A g^{-1} current rate, the Sb_2S_3/SGS anode reaches a high specific capacity of 792.8 mA h g^{-1} after 90 cycles (see **Figure 2F**). After 900 cycles at a higher current rate of 2 A g^{-1} (in **Figure 2G**), the Sb_2S_3/SGS anode still has an excellent cycle life, and the capacity retention rate is ~83%.

Sb_2S_3/M_xS_y Composites

Most metal sulfides (M_xS_y) have hierarchical structures, and Na^+ can easily move in the interlayers of metal sulfides without damaging their hierarchical structures (Tao et al., 2021). Thus, the use of binary metal sulfides to construct heterostructures to reduce the huge internal stress of alloy-based anodes and maintain the integrity of nanostructures has attracted extensive attention (Wang et al., 2018; Lin et al., 2021; Wang et al., 2019a). In this context, common metal sulfides (M_xS_y), including SnS_2 (Wang et al., 2018), ZnS (Dong et al., 2017), FeS_2 (Cao et al., 2020), In_2S_3 (Huang et al., 2018), and Bi_2S_3 (Li et al., 2021), have been combined with Sb_2S_3 as anode materials of SIBs.

For example, a composite of multiwalled carbon nanotubes (MCNTs) and In_2S_3-Sb_2S_3 particles (denoted as I-S@MCNTs) with a unique morphology of formicary microspheres was formed to solve the poor cycling stability and rate performance of SIBs (Huang et al., 2018). As shown in **Supplementary Figure S3A**, the hierarchical spheres are assembled by crumpled nanosheets (5–8 nm), which significantly shorten the diffusion path and accelerate the transport rate of Na^+. Similarly, Wang D. et al. (2021) designed an armored hydrangea-like Sb_2S_3/MoS_2 heterostructure composite (denoted as SMS@C) as a superior SIB anode material (**Supplementary Figure S3B**). After 650 cycles at a higher current density of 5 A g^{-1}, the SMS@C anode exhibited an enhanced cycling performance of 411.5 mA h g^{-1} (**Supplementary Figure S3E**). Additionally, Dong et al. (2017) designed a polyhedron composite (~1.5 μm) with a ZnS inner-core structure and Sb_2S_3/C double-shell structure (ZnS-Sb_2S_3@C), capitalizing on full advantages of the zeolitic imidazolate framework (ZIF-8). The structure of ZnS-Sb_2S_3@C core-double shell composites had enough space to greatly adapt to the volume expansion during the repeated insertion/extraction of Na^+, and exhibited a superior reversible capacity of 630 mA h g^{-1} at a current density of 0.1 A g^{-1} after 120 cycles with a high Coulombic efficiency of ~100% (**Supplementary Figures S3C,F**).

Recently, a breakthrough about Sb_2S_3@FeS_2 hollow nanorods used as high-performance SIB electrode materials was reported. Cao et al. (2020) embedded Sb_2S_3@FeS_2 hollow nanorods (SFS) into a nitrogen-doped graphene matrix, and synthesized Sb_2S_3@FeS_2/N-doped graphene composite (denoted as SFS/C) *via* a simple two-step solvothermal synthesis technique

(**Supplementary Figures S3D,G**). The clever design of the heterostructure extremely accelerated the Na^+ transport, and greatly alleviated the volume expansion under long-period performance (1,000 cycles) (Wu et al., 2019a; Wu et al., 2019b; Liu et al., 2022). The SFS/C anode displayed a superior reversible capacity of 725.4 mA h g^{-1} after 90 cycles at 0.1 A g^{-1} (see **Supplementary Figure S3H**). When tested even at 5 A g^{-1}, the SFS/C anode had an excellent cycle performance with a capacity retention of ~85.7% after 1,000 cycles (**Supplementary Figure S3I**).

Other Composites

In addition to the aforementioned Sb_2S_3-based nanomaterials, polypyrrole (PPy) (Wang et al., 2016; Zheng et al., 2018), MXene ($M_{n+1}X_nT_x$, where M is the early transition metal, X represents C/N, and T_x is the surface functional group (-O, -OH or -F), n = 0,1,2,3,4. e.g., $Ti_3C_2T_x$, Ti_3C_2) (Wang et al., 2019b; Zhang H. et al., 2021; He et al., 2021), and metal oxides (e.g., SnO_2) (Chang et al., 2020a) can also be combined with Sb_2S_3 to fabricate better SIB anodes.

For instance, Shi et al. (Yin et al., 2019) prepared Sb_2S_3/meso@microporous carbon nanofibers@polypyrrole composites (denoted as Sb_2S_3/MMCN@PPy) though a novel multi-step method combining polymerization, sulfidation and solvothermal process (**Supplementary Figure S4A**). SEM image of Sb_2S_3/MMCN@PPy composites is shown in **Supplementary Figure S4B**. When investigated as SIB anode, Sb_2S_3/MMCN@PPy composite exhibited a discharge capacity of 535.3 mA h g^{-1} at a current density of 100 mA g^{-1}, and the discharge specific capacity could recover to 446 mA h g^{-1} after 50 cycles when returned to 100 mA g^{-1} current rate (**Supplementary Figure S4C**). Shi et al. (2019) synthesized Sb_2S_3@PPy coaxial nanorods *via* a hydrothermal method. When tested at 100 mA g^{-1}, it showed a superior reversible capacity as high as 881 mA h g^{-1} after 50 cycles, which was higher than those reported of MWNTs@Sb_2S_3@PPy composites (Wang et al., 2016), flower-like Sb_2S_3/PPy microspheres (Zheng et al., 2018), and Sb_2S_3/MMCN@PPy composites (Yin et al., 2019).

Furthermore, MXene is considered as an outstanding matrix because of the effective diffusion and mobility for Na^+ and excellent electronic conductivity. $Ti_3C_2T_x$ is one of the most studied MXene materials, and the theoretical capacity is 352 mA h g^{-1} when used as the anode of SIBs (Zhang H. et al., 2021; He et al., 2021; Ren et al., 2021). For instance, Zhang H. et al. (2021); Ren et al. (2021) prepared Sb_2S_3@$Ti_3C_2T_x$ composite and Sb_2S_3@m-$Ti_3C_2T_x$ composite by a wet chemical method, in which Sb_2S_3 nanoparticles were *in situ* nucleated and grown uniformly on the surface of $Ti_3C_2T_x$ nanosheets. It was found that $Ti_3C_2T_x$, as a conductive skeleton, could effectively alleviate the volume expansion of Sb_2S_3 during charge/discharge progress. In 2021, inspired by the stomatal structure from natural leaves, He et al. (2021) successfully synthesized Sb_2S_3/nitrogen-doped Ti_3C_2 composites (denoted as L-Sb_2S_3/Ti_3C_2) *via* a solvothermal method (**Supplementary Figure S4D**). L-Sb_2S_3/Ti_3C_2 composite showed a unique elm leaf-like morphology in **Supplementary Figure S4E**, with a length of 60–80 nm and a width of 30–40 nm, respectively. When used as SIB anode, L-Sb_2S_3/Ti_3C_2 composite displayed a high capacity of 502.2 mA h g^{-1} at a current rate of 100 mA g^{-1} from 0.01 to 3 V (**Supplementary Figure S4F**).

CONCLUSION AND OUTLOOK

In this review, we briefly summarize the applications of Sb_2S_3-based nanomaterials for high-performance SIBs, mainly including Sb_2S_3, Sb_2S_3/carbon composites, Sb_2S_3/graphene composites, Sb_2S_3/M_xS_y composites, and other related composites. Although many significant works have been made in SIBs, there are still some problems that need to be solved, and we propose some possible directions for the anode research of SIBs in the future:

1) During the charge/discharge cycles, Sb_2S_3 nanoparticles are easy to accumulate because of their high surface activity energy. This results in a significant volume change and capacity declining. Therefore, it is necessary to design and fabricate more reasonable nanostructures, such as hierarchical hollow nanotubes or hierarchical spheres (Xie F. et al., 2019), to fully buffer the strain of volume change and further improve the cycling performance. In addition, some soft materials could be added to improve the flexibility, so as to avoid the collapse of the anode due to the volume expansion.

2) Carbonaceous materials are often the main choice to combine with Sb_2S_3 to build dense conductive physical barriers. However, the content of Sb_2S_3 and the corresponding specific capacity of composite materials are reduced. Therefore, the carbon content should be optimized so that the Sb_2S_3-based materials achieve better electrochemical performance. In addition, Sb_2S_3/carbonaceous composites fabricated by traditional synthesis techniques suffer from the poor mechanical adhesion and high interface resistance between Sb_2S_3 and carbonaceous materials. It is highly desirable to optimize the preparation methods and explore more carbonaceous materials (e.g., biochar, amorphous carbon) to establish compact conductive physical barriers to further enhance the electrochemical performance of Sb_2S_3-based materials.

3) Until now, the cycle lives of many Sb_2S_3-based materials have been tested at room temperature. In order to satisfy the demands of different applications, it is very urgent to explore Sb_2S_3-based anode materials that can cycle under either higher temperature (up to 60 °C) or lower (−20°C).

4) The mechanism of Na^+ storage in Sb_2S_3-based nanomaterials and the phase changes during repeated charging/discharging still need to be explored. Operating technologies, such as *in situ* X-ray technology, *in situ* scanning probe microscopy, technologies based on synchronized X-rays, as well as *in situ* electron microscopy, are very helpful in acquiring time-related information and studying the mechanism of Na^+ storage of Sb_2S_3-based nanomaterials. Therefore, more research using operating technology is needed to deeply understand Sb_2S_3-based electrode nanomaterials used in SIBs.

AUTHOR CONTRIBUTIONS

YL and GW conceived the idea. MG and GW wrote the draft. All authors contributed to the writing, discussion, and revision of the final version of the article.

FUNDING

This work was financially supported by the Chinese 02 Special Fund (Grant No.2017ZX02408003) and the Chinese 1000 Plan for High Level Foreign Experts (Grant No. WQ20154100278).

SUPPLEMENTARY MATERIAL

The Supplementary Material for this article can be found online at: https://www.frontiersin.org/articles/10.3389/fchem.2022.870564/full#supplementary-material

Supplementary Figure S1 | (A) SEM image of α-Sb_2S_3 nanoparticles; **(B)** cycle performance of α-Sb_2S_3 at 0.05 A g^{-1}; **(C)** SEM image of the few-layer 2D-Sb_2S_3 nanosheets; **(D)** cyclic capacity of 2D-SS measured at 0.2 A g^{-1}; **(E)** SEM image of Sb_2S_3 hollow microspheres; **(F)** cycling performances of three experimental Sb_2S_3 electrodes at 1A g^{-1}; (g) SEM and TEM images of multi-shell Sb_2S_3; **(H)** comparison of the rate performance of multi-shell Sb_2S_3, single-shell Sb_2S_3, and pristine Sb_2S_3. **(A,B)** Adapted with permission from Hwang et al. (2016). Copyright 2013, The Royal Society of Chemistry. **(C,D)** Adapted with permission from Yao et al. (2019). Copyright 2018, Elsevier. **(E,F)** Adapted with permission from Xie et al. (2018). Copyright 2018, Springer. **(G,H)** Adapted with permission from Xie et al. (2019a). Copyright 2019, Elsevier.

Supplementary Figure S2 | (A) SEM image of Sb_2S_3@C rods; **(B)** cycle performance of Sb_2S_3@C rods at 0.1 A g^{-1}; **(C)** SEM image of SS/CFC; **(D)** cycle performances of SS/CFC and SS powder at 0.5 A g^{-1}; **(E)** SEM image of SS/Sb@C nanocomposites; **(F)** cycling performances of SS/Sb@C and Sb_2S_3 nanocomposites at 0.1 A g^{-1}. **(A,B)** Adapted with permission from Hongshuai Hou et al. (2015). Copyright 2015, American Chemical Society. **(C,D)** Adapted with permission from Liu et al. (2017). Copyright 2017, The Royal Society of Chemistry. **(E,F)** Adapted with permission from Zhao et al. (2020). Copyright 2020, The Royal Society of Chemistry.

Supplementary Figure S3 | SEM images: **(A)** In_2S_3-Sb_2S_3@MCNTs microsphere, **(B)** Sb_2S_3/MoS_2@C composite (SMS@C), **(C)** ZnS-Sb_2S_3@C polyhedron, and **(D)** Sb_2S_3@FeS_2/N-graphene composite (SFS/C); **(E)** sodium storage properties of the SMS@C and SMS heterostructure at 5 A g^{-1}; **(F)** rate capability of ZnS-Sb_2S_3@C core-shell SIB anode; **(G)** schematic illustration of the fabrication process of the SFS/C composite; (h) charge capability of the SFS/C anode at various rates; **(I)** cycle performances of Sb_2S_3, SFS, and SFS/C composites at a high rate of 5 A g^{-1}. **(A)** Adapted with permission from Huang et al. (2018). Copyright 2018, Wiley-VCH. **(B, E)** Adapted with permission from Wang et al. (2021a). Copyright 2021, Elsevier. **(c,f)** Adapted with permission from Dong et al. (2017). Copyright 2017, American Chemical Society. **(D,G–I)** Adapted with permission from Cao et al. (2020). Copyright 2020, American Chemical Society.

Supplementary Figure S4 | (A) Schematic diagram of the formation process of the Sb_2S_3/MMCN@PPy composite; **(B)** SEM image of Sb_2S_3/MMCN@PPy composite; **(C)** rate capability performances of pure Sb_2S_3 and Sb_2S_3/MMCN@PPy composite; **(D)** schematic illustration of the synthetic process of L-Sb_2S_3/Ti_3C_2 composite; **(E)** SEM image of L-Sb_2S_3/Ti_3C_2 composite; **(F)** Rate capability performances of Sb_2S_3, Sb_2S_3/Ti_3C_2, and L-Sb_2S_3/Ti_3C_2. **(A–C)** Adapted with permission from Yin et al. (2019). Copyright 2019, Elsevier. **(D–F)** Adapted with permission from He et al. (2021). Copyright 2021, Science China Press and Springer-Verlag GmbH Germany, part of Springer Nature.

REFERENCES

Bag, S., Roy, A., and Mitra, S. (2019). Sulfur, Nitrogen Dual Doped Reduced Graphene Oxide Supported Two-Dimensional Sb 2 S 3 Nanostructures for the Anode Material of Sodium-Ion Battery. *ChemistrySelect* 4 (22), 6679–6686. doi:10.1002/slct.201901153

Cao, L., Gao, X., Zhang, B., Ou, X., Zhang, J., and Luo, W.-B. (2020). Bimetallic Sulfide Sb2S3@FeS2 Hollow Nanorods as High-Performance Anode Materials for Sodium-Ion Batteries. *ACS Nano* 14 (3), 3610–3620. doi:10.1021/acsnano.0c00020

Chang, G., Yin, X., Shi, S., Zhao, Y., and Zhang, J. (2020a). Sb2S3@SnO2 Hetero-Nanocomposite as High-Performance Anode Material for Sodium-Ion Battery. *Int. J. Green Energ.* 17 (15), 1044–1050. doi:10.1080/15435075.2020.1821692

Chang, G., Yin, X., Shi, S., Zhao, Y., and Zhang, J. (2020b). Sb2S3@YP Nanostructured Anode Material Synthesized by a Novel Vaporization-Condensation Method for Long Cycle-Life Sodium-Ion Battery. *J. Electrochem. Soc.* 167 (14), 140531. doi:10.1149/1945-7111/abc658

Choi, J.-H., Ha, C.-W., Choi, H.-Y., Shin, H.-C., and Lee, S.-M. (2017). High Performance Sb2S3/carbon Composite with Tailored Artificial Interface as an Anode Material for Sodium Ion Batteries. *Met. Mater. Int.* 23 (6), 1241–1249. doi:10.1007/s12540-017-7105-y

Choi, J.-H., Ha, C.-W., Choi, H.-Y., Shin, H.-C., Park, C.-M., Jo, Y.-N., et al. (2016). Sb2S3 Embedded in Amorphous P/C Composite Matrix as High-Performance Anode Material for Sodium Ion Batteries. *Electrochimica Acta* 210, 588–595. doi:10.1016/j.electacta.2016.05.190

Chong, W. G., Xiao, Y., Huang, J.-Q., Yao, S., Cui, J., Qin, L., et al. (2018). Highly Conductive Porous Graphene/sulfur Composite Ribbon Electrodes for Flexible Lithium-Sulfur Batteries. *Nanoscale* 10 (45), 21132–21141. doi:10.1039/c8nr06666c

Cui, J., Yao, S., Lu, Z., Huang, J.-Q., Chong, W. G., Ciucci, F., et al. (2018). Revealing Pseudocapacitive Mechanisms of Metal Dichalcogenide SnS2 / Graphene-CNT Aerogels for High-Energy Na Hybrid Capacitors. *Adv. Energ. Mater.* 8 (10), 1702488. doi:10.1002/aenm.201702488

Dashairya, L., Das, D., and Saha, P. (2021). Elucidating the Role of Graphene and Porous Carbon Coating on Nanostructured Sb2S3 for superior Lithium and Sodium Storage. *J. Alloys Comp.* 883, 160906–160913. doi:10.1016/j.jallcom.2021.160906

Dashairya, L., and Saha, P. (2020). Antimony Sulphide Nanorods Decorated onto Reduced Graphene Oxide Based Anodes for Sodium-Ion Battery. *Mater. Today Proc.* 21, 1899–1904. doi:10.1016/j.matpr.2020.01.247

Deng, M., Li, S., Hong, W., Jiang, Y., Xu, W., Shuai, H., et al. (2019). Natural Stibnite Ore (Sb2S3) Embedded in Sulfur-Doped Carbon Sheets: Enhanced Electrochemical Properties as Anode for Sodium Ions Storage. *RSC Adv.* 9 (27), 15210–15216. doi:10.1039/c9ra02301a

Deng, P., Yang, J., He, W., Li, S., Zhou, W., Tang, D., et al. (2018). Tin-Assisted Sb2S3Nanoparticles Uniformly Grafted on Graphene Effectively Improves Sodium-Ion Storage Performance. *ChemElectroChem* 5 (5), 811–816. doi:10.1002/celc.201800016

Dong, S., Li, C., Ge, X., Li, Z., and Yin, X. L. (2017). ZnS-Sb2S3@C Core-Double Shell Polyhedron Structure Derived from Metal-Organic Framework as Anodes for High Performance Sodium Ion Batteries. *Acs Nano* 11 (6), 6474–6482. doi:10.1021/acsnano.7b03321

Dong, Y., Hu, M., Zhang, Z., Zapien, J. A., Wang, X., Lee, J.-M., et al. (2019). Nitrogen-Doped Carbon-Encapsulated Antimony Sulfide Nanowires Enable High Rate Capability and Cyclic Stability for Sodium-Ion Batteries. *ACS Appl. Nano Mater.* 2 (3), 1457–1465. doi:10.1021/acsanm.8b02335

Fan, T.-E., and Xie, H.-F. (2019). Sb2S3-rGO for High-Performance Sodium-Ion Battery Anodes on Al and Cu Foil Current Collector. *J. Alloys Comp.* 775, 549–553. doi:10.1016/j.jallcom.2018.10.103

Fang, L., Lan, Z., Guan, W., Zhou, P., Bahlawane, N., Sun, W., et al. (2019). Hetero-interface Constructs Ion Reservoir to Enhance Conversion Reaction Kinetics for Sodium/lithium Storage. *Energ. Storage Mater.* 18, 107–113. doi:10.1016/j.ensm.2018.10.002

Fu, L., Shang, C., Li, G., Hu, L., Zhang, X., Huang, L., et al. (2019). Lithium Pre-cycling Induced Fast Kinetics of Commercial Sb 2 S 3 Anode for Advanced Sodium Storage. *Energy Environ. Mater.* 2 (3), 209–215. doi:10.1002/eem2.12037

Ge, P., Hou, H., Ji, X., Huang, Z., Li, S., and Huang, L. (2018). Enhanced Stability of Sodium Storage Exhibited by Carbon Coated Sb2S3 Hollow Spheres. *Mater. Chem. Phys.* 203, 185–192. doi:10.1016/j.matchemphys.2017.10.003

Ge, P., Zhang, L., Zhao, W., Yang, Y., Sun, W., and Ji, X. (2020). Interfacial Bonding of Metal-Sulfides with Double Carbon for Improving Reversibility of Advanced Alkali-Ion Batteries. *Adv. Funct. Mater.* 30 (16), 1910599. doi:10.1002/adfm.201910599

Guo, D., Yang, M., Li, Y., Xue, Y., Liu, G., Wu, N., et al. (2020). Hydrogel-derived VPO4/porous Carbon Framework for Enhanced Lithium and Sodium Storage. *Nanoscale* 12 (6), 3812–3819. doi:10.1039/d0nr00460j

Guo, D., Yang, M., Zhang, L., Li, Y., Wang, J., Liu, G., et al. (2019). Cr2O3 Nanosheet/carbon Cloth Anode with strong Interaction and Fast Charge Transfer for Pseudocapacitive Energy Storage in Lithium-Ion Batteries. *RSC Adv.* 9 (57), 33446–33453. doi:10.1039/c9ra07465a

Hao, X., Zhao, Q., Su, S., Zhang, S., Ma, J., Shen, L., et al. (2019). Constructing Multifunctional Interphase between Li 1.4 Al 0.4 Ti 1.6 (PO 4) 3 and Li Metal by Magnetron Sputtering for Highly Stable Solid-State Lithium Metal Batteries. *Adv. Energ. Mater.* 9 (34), 1901604. doi:10.1002/aenm.201901604

He, F., Tang, C., Zhu, G., Liu, Y., Du, A., Zhang, Q., et al. (2021). Leaf-inspired Design of Mesoporous Sb2S3/N-Doped Ti3C2Tx Composite towards Fast Sodium Storage. *Sci. China Chem.* 64 (6), 964–973. doi:10.1007/s11426-020-9942-9

Hou, H., Jing, M., Huang, Z., Yang, Y., Zhang, Y., Chen, J., et al. (2015). One-Dimensional Rod-like Sb2S3-Based Anode for High-Performance Sodium-Ion Batteries. *ACS Appl. Mater. Inter.* 7 (34), 19362–19369. doi:10.1021/acsami.5b05509

Huang, Y., Wang, Z., Jiang, Y., Li, S., Wang, M., Ye, Y., et al. (2018). Conductivity and Pseudocapacitance Optimization of Bimetallic Antimony-Indium Sulfide Anodes for Sodium-Ion Batteries with Favorable Kinetics. *Adv. Sci.* 5 (10), 1800613. doi:10.1002/advs.201800613

Hwang, S. M., Kim, J., Kim, Y., and Kim, Y. (2016). Na-ion Storage Performance of Amorphous Sb2S3nanoparticles: Anode for Na-Ion Batteries and Seawater Flow Batteries. *J. Mater. Chem. A.* 4 (46), 17946–17951. doi:10.1039/c6ta07838a

Jaramillo-Quintero, O. A., Barrera-Peralta, R. V., El Hachimi, A. G., Guillén-López, A., Pérez, O., Reguera, E., et al. (2021). Understanding the Interaction between Heteroatom-Doped Carbon Matrix and Sb2S3 for Efficient Sodium-Ion Battery Anodes. *J. Colloid Interf. Sci.* 585, 649–659. doi:10.1016/j.jcis.2020.10.044

Jiang, Q., Zhang, W.-q., Zhao, J.-c., Rao, P.-h., and Mao, J.-f. (2021). Superior Sodium and Lithium Storage in Strongly Coupled Amorphous Sb2S3 Spheres and Carbon Nanotubes. *Int. J. Miner Metall. Mater.* 28 (7), 1194–1203. doi:10.1007/s12613-021-2259-5

Jin Pan, Z.-L. Z., Deng, J.-Q., Wang, J., Fang, C.-C., and Yao, Q.-R. (2017). Template-free Synthesis of Sb2S3 Micro Tubes as the Anode Materials for Sodium-Ion Batteries. *ADVANCED MATERIALS ENERGY SUSTAINABILITY*, 81–89. doi:10.1142/9789813220393_0010

Kravchyk, K. V., Kovalenko, M. V., and Bodnarchuk, M. I. (2020). Colloidal Antimony Sulfide Nanoparticles as a High-Performance Anode Material for Li-Ion and Na-Ion Batteries. *Sci. Rep.* 10 (1), 2554–2561. doi:10.1038/s41598-020-59512-3

Li, C.-Y., Patra, J., Yang, C.-H., Tseng, C.-M., Majumder, S. B., Dong, Q.-F., et al. (2017a). Electrolyte Optimization for Enhancing Electrochemical Performance of Antimony Sulfide/Graphene Anodes for Sodium-Ion Batteries-Carbonate-Based and Ionic Liquid Electrolytes. *ACS Sust. Chem. Eng.* 5 (9), 8269–8276. doi:10.1021/acssuschemeng.7b01939

Li, J., Yan, D., Zhang, X., Hou, S., Li, D., Lu, T., et al. (2017b). *In Situ* growth of Sb2S3 on Multiwalled Carbon Nanotubes as High-Performance Anode Materials for Sodium-Ion Batteries. *Electrochimica Acta* 228, 436–446. doi:10.1016/j.electacta.2017.01.114

Li, K., Liu, X., Qin, Y., Zhao, Z., Xu, Y., Yi, Y., et al. (2021). Sb2S3-Bi2S3 Microrods with the Combined Action of Carbon Encapsulation and rGO Confinement for Improving High Cycle Stability in Sodium/potassium Storage. *Chem. Eng. J.* 414, 128787–128795. doi:10.1016/j.cej.2021.128787

Li, M., Huang, F., Pan, J., Li, L., Zhang, Y., Yao, Q., et al. (2019). Amorphous Sb2S3 Nanospheres *In-Situ* Grown on Carbon Nanotubes: Anodes for NIBs and KIBs. *Nanomaterials* 9 (9), 1323. doi:10.3390/nano9091323

Li, P., Jeong, J. Y., Jin, B., Zhang, K., and Park, J. H. (2020). Large and Reversible Sodium Storage through Interlaced Reaction Design. *Energ. Storage Mater.* 25, 687–694. doi:10.1016/j.ensm.2019.09.018

Li, P., Wang, P., Zheng, X., Yu, H., Qian, S., Shui, M., et al. (2015). Enhanced Sodium Storage Property of Copper Nitrate Hydrate by Carbon Nanotube. *J. Electroanalytical Chem.* 755, 92–99. doi:10.1016/j.jelechem.2015.07.043

Li, Y. X., Zhai, X. L., Liu, Y., Wei, H. J., Ma, J. Q., Chen, M., et al. (2020). WO3-Based Materials as Electrocatalysts for Hydrogen Evolution Reaction. *Frontiers in Materials* 7, 105. doi:10.3389/fmats.2020.00105

Lin, J., Yao, L., Zhang, C., Ding, H., Yuanhui, W., Li, S., et al. (2021). Construction of Sb2S3@SnS@C Tubular Heterostructures as High-Performance Anode Materials for Sodium-Ion Batteries. *ACS Sust. Chem. Eng.* 9 (33), 11280–11289. doi:10.1021/acssuschemeng.1c04497

Liu, G., Cui, J., Luo, R., Liu, Y., Huang, X., Wu, N., et al. (2019a). 2D MoS2 Grown on Biomass-Based Hollow Carbon Fibers for Energy Storage. *Appl. Surf. Sci.* 469, 854–863. doi:10.1016/j.apsusc.2018.11.067

Liu, G., Li, M., Wu, N., Cui, L., Huang, X., Liu, X., et al. (2018a). Single-Crystalline Particles: An Effective Way to Ameliorate the Intragranular Cracking, Thermal Stability, and Capacity Fading of the LiNi0.6Co0.2Mn0.2O2 Electrodes. *J. Electrochem. Soc.* 165 (13), A3040–A3047. doi:10.1149/2.0491813jes

Liu, G., Xu, L., Li, Y., Guo, D., Wu, N., Yuan, C., et al. (2022). Metal-organic Frameworks Derived Anatase/rutile Heterostructures with Enhanced Reaction Kinetics for Lithium and Sodium Storage. *Chem. Eng. J.* 430, 132689. doi:10.1016/j.cej.2021.132689

Liu, Q., Wang, H., Jiang, C., and Tang, Y. (2019b). Multi-ion Strategies towards Emerging Rechargeable Batteries with High Performance. *Energ. Storage Mater.* 23, 566–586. doi:10.1016/j.ensm.2019.03.028

Liu, S., Cai, Z., Zhou, J., Zhu, M., Pan, A., and Liang, S. (2017). High-performance Sodium-Ion Batteries and Flexible Sodium-Ion Capacitors Based on Sb2X3(X = O, S)/carbon Fiber Cloth. *J. Mater. Chem. A.* 5 (19), 9169–9176. doi:10.1039/c7ta01895a

Liu, X., Du, Y., Xu, X., Zhou, X., Dai, Z., and Bao, J. (2016). Enhancing the Anode Performance of Antimony through Nitrogen-Doped Carbon and Carbon Nanotubes. *J. Phys. Chem. C* 120 (6), 3214–3220. doi:10.1021/acs.jpcc.5b11926

Liu, Y., Wang, Y., Wang, F., Lei, Z., Zhang, W., Pan, K., et al. (2019c). Facile Synthesis of Antimony Tungstate Nanosheets as Anodes for Lithium-Ion Batteries. *Nanomaterials* 9 (12), 1689. doi:10.3390/nano9121689

Liu, Y., Wei, H., Zhai, X., Wang, F., Ren, X., Xiong, Y., et al. (2021). Graphene-based Interlayer for High-Performance Lithium-Sulfur Batteries: A Review. *Mater. Des.* 211, 110171. doi:10.1016/j.matdes.2021.110171

Liu, Z., Song, T., and Paik, U. (2018b). Sb-based Electrode Materials for Rechargeable Batteries. *J. Mater. Chem. A.* 6 (18), 8159–8193. doi:10.1039/c8ta01782d

Lv, W., Li, Z., Deng, Y., Yang, Q.-H., and Kang, F. (2016). Graphene-based Materials for Electrochemical Energy Storage Devices: Opportunities and Challenges. *Energ. Storage Mater.* 2, 107–138. doi:10.1016/j.ensm.2015.10.002

Ma, J., Wei, H., Liu, Y., Ren, X., Li, Y., Wang, F., et al. (2020). Application of Co3O4-Based Materials in Electrocatalytic Hydrogen Evolution Reaction: A Review. *Int. J. Hydrogen Energ.* 45 (41), 21205–21220. doi:10.1016/j.ijhydene.2020.05.280

Mullaivananathan, V., and Kalaiselvi, N. (2019). Sb2S3 Added Bio-Carbon: Demonstration of Potential Anode in Lithium and Sodium-Ion Batteries. *Carbon* 144, 772–780. doi:10.1016/j.carbon.2019.01.001

Pan, J., Zuo, Z., Deng, J., Yao, Q., Wang, Z., and Zhou, H. (2018a). Sb 2 S 3 Single crystal Nanowires with Comparable Electrochemical Properties as an Anode for Sodium Ion Batteries. *Surf. Inter.* 10, 170–175. doi:10.1016/j.surfin.2017.10.010

Pan, Z.-Z., Yan, Y., Cui, N., Xie, J.-C., Zhang, Y.-B., Mu, W.-S., et al. (2018b). Ionic Liquid-Assisted Preparation of Sb2S3/Reduced Graphene Oxide Nanocomposite for Sodium-Ion Batteries. *Adv. Mater. Inter.* 5 (5), 1701481. doi:10.1002/admi.201701481

Pang, P., Wang, Z., Tan, X., Deng, Y., Nan, J., Xing, Z., et al. (2019). LiCoO2@LiNi0.45Al0.05Mn0.5O2 as High-Voltage Lithium-Ion Battery Cathode Materials with Improved Cycling Performance and thermal Stability. *Electrochimica Acta* 327, 135018–135026. doi:10.1016/j.electacta.2019.135018

Qin, L., Zhai, D., Lv, W., Yang, W., Huang, J., Yao, S., et al. (2017). A High-Performance Lithium Ion Oxygen Battery Consisting of Li2O2 Cathode and Lithiated Aluminum Anode with Nafion Membrane for Reduced O2 Crossover. *Nano Energy* 40, 258–263. doi:10.1016/j.nanoen.2017.08.029

Ren, M., Cao, D., Jiang, W., Su, K., Pan, L., Jiang, Y., et al. (2021). Hierarchical Composite of Sb2S3 Decorated on Highly Crumpled Ti3C2Tx Nanosheets for

Enhanced Sodium Storage Properties. *Electrochimica Acta* 373, 137835–137844. doi:10.1016/j.electacta.2021.137835

Schmuch, R., Wagner, R., Hörpel, G., Placke, T., and Winter, M. (2018). Performance and Cost of Materials for Lithium-Based Rechargeable Automotive Batteries. *Nat. Energ.* 3 (4), 267–278. doi:10.1038/s41560-018-0107-2

Shan, Y., Li, Y., and Pang, H. (2020). Applications of Tin Sulfide-Based Materials in Lithium-Ion Batteries and Sodium-Ion Batteries. *Adv. Funct. Mater.* 30 (23), 2001298. doi:10.1002/adfm.202001298

Shi, F., Chen, C., and Xu, Z.-L. (2021). Recent Advances on Electrospun Nanofiber Materials for Post-lithium Ion Batteries. *Adv. Fiber Mater.* 3 (5), 275–301. doi:10.1007/s42765-021-00070-2

Shi, Y., Li, F., Zhang, Y., He, L., Ai, Q., and Luo, W. (2019). Sb2S3@PPy Coaxial Nanorods: A Versatile and Robust Host Material for Reversible Storage of Alkali Metal Ions. *Nanomaterials* 9 (4), 560–571. doi:10.3390/nano9040560

Sui, D., Chang, M., Peng, Z., Li, C., He, X., Yang, Y., et al. (2021a). Graphene-Based Cathode Materials for Lithium-Ion Capacitors: A Review. *Nanomaterials* 11 (10), 2771. doi:10.3390/nano11102771

Sui, D., Xu, L., Zhang, H., Sun, Z., Kan, B., Ma, Y., et al. (2020). A 3D Cross-Linked Graphene-Based Honeycomb Carbon Composite with Excellent Confinement Effect of Organic Cathode Material for Lithium-Ion Batteries. *Carbon* 157, 656–662. doi:10.1016/j.carbon.2019.10.106

Sui, Y., Zhou, J., Wang, X., Wu, L., Zhong, S., and Li, Y. (2021b). Recent Advances in Black-Phosphorus-Based Materials for Electrochemical Energy Storage. *Mater. Today* 42, 117–136. doi:10.1016/j.mattod.2020.09.005

Tao, F., Liu, Y., Ren, X., Jiang, A., Wei, H., Zhai, X., et al. (2021). Carbon Nanotube-Based Nanomaterials for High-Performance Sodium-Ion Batteries: Recent Advances and Perspectives. *J. Alloys Comp.* 873, 159742. doi:10.1016/j.jallcom.2021.159742

Tao, F., Liu, Y., Ren, X., Wang, J., Zhou, Y., Miao, Y., et al. (2022). Different Surface Modification Methods and Coating Materials of Zinc Metal Anode. *J. Energ. Chem.* 66, 397–412. doi:10.1016/j.jechem.2021.08.022

Wang, D., Cao, L., Luo, D., Gao, R., Li, H., Wang, D., et al. (2021a). Chain Mail Heterostructured Hydrangea-like Binary Metal Sulfides for High Efficiency Sodium Ion Battery. *Nano Energy* 87, 106185. doi:10.1016/j.nanoen.2021.106185

Wang, F., Feng, T., Jin, X., Zhou, Y., Xu, Y., Gao, Y., et al. (2021b). Atomic Co/Ni Active Sites Assisted MOF-Derived Rich Nitrogen-Doped Carbon Hollow Nanocages for Enhanced Lithium Storage. *Chem. Eng. J.* 420, 127583. doi:10.1016/j.cej.2020.127583

Wang, F., Liu, Y., Wei, H.-J., Li, T.-F., Xiong, X.-H., Wei, S.-Z., et al. (2021c). Recent Advances and Perspective in Metal Coordination Materials-Based Electrode Materials for Potassium-Ion Batteries. *Rare Met.* 40 (2), 448–470. doi:10.1007/s12598-020-01649-1

Wang, F., Liu, Y., Zhao, Y., Wang, Y., Wang, Z., Zhang, W., et al. (2017). Facile Synthesis of Two-Dimensional Porous MgCo2O4 Nanosheets as Anode for Lithium-Ion Batteries. *Appl. Sci.* 8 (1), 22. doi:10.3390/app8010022

Wang, G., Chen, C., Chen, Y., Kang, X., Yang, C., Wang, F., et al. (2020). Self-Stabilized and Strongly Adhesive Supramolecular Polymer Protective Layer Enables Ultrahigh-Rate and Large-Capacity Lithium-Metal Anode. *Angew. Chem. Int. Ed.* 59 (5), 2055–2060. doi:10.1002/anie.201913351

Wang, S., Liu, S., Li, X., Li, C., Zang, R., Man, Z., et al. (2018). SnS 2 /Sb 2 S 3 Heterostructures Anchored on Reduced Graphene Oxide Nanosheets with Superior Rate Capability for Sodium-Ion Batteries. *Chem. Eur. J.* 24 (15), 3873–3881. doi:10.1002/chem.201705855

Wang, S., Yuan, S., Yin, Y.-B., Zhu, Y.-H., Zhang, X.-B., and Yan, J.-M. (2016). Green and Facile Fabrication of MWNTs@Sb2S3@PPy Coaxial Nanocables for High-Performance Na-Ion Batteries. *Part. Part. Syst. Charact.* 33 (8), 493–499. doi:10.1002/ppsc.201500227

Wang, P. Y., Pu, Z. H., Li, W. Q., Zhu, J. W., Zhang, C. T., and Zhao, Y. F. (2019a). Coupling NiSe2-Ni2P Heterostructure Nanowrinkles for Highly Efficient Overall Water Splitting. *Journal of Catalysis* 377, 600–608. doi:10.1016/j.jcat.2019.08.005

Wang, X., Huang, R.-q., Niu, S.-z., Xu, L., Zhang, Q.-c., Amini, A., et al. (2021d). Research Progress on Graphene-Based Materials for High-Performance Lithium-Metal Batteries. *New Carbon Mater.* 36 (4), 711–728. doi:10.1016/s1872-5805(21)60081-1

Wang, X., Yang, C., Xiong, X., Chen, G., Huang, M., Wang, J.-H., et al. (2019b). A Robust Sulfur Host with Dual Lithium Polysulfide Immobilization Mechanism for Long Cycle Life and High Capacity Li-S Batteries. *Energ. Storage Mater.* 16, 344–353. doi:10.1016/j.ensm.2018.06.015

Wen, S., Zhao, J., Zhao, Y., Xu, T., and Xu, J. (2019). Reduced Graphene Oxide (RGO) Decorated Sb2S3 Nanorods as Anode Material for Sodium-Ion Batteries. *Chem. Phys. Lett.* 716, 171–176. doi:10.1016/j.cplett.2018.12.031

Wu, F., Guo, X., Li, M., and Xu, H. (2017). One-step Hydrothermal Synthesis of Sb 2 S 3 /reduced Graphene Oxide Nanocomposites for High-Performance Sodium Ion Batteries Anode Materials. *Ceramics Int.* 43 (8), 6019–6023. doi:10.1016/j.ceramint.2017.01.141

Wu, N., Qiao, X., Shen, J., Liu, G., Sun, T., Wu, H., et al. (2019a). Anatase Inverse Opal TiO2-x@N-Doped C Induced the Dominant Pseudocapacitive Effect for Durable and Fast Lithium/sodium Storage. *Electrochimica Acta* 299, 540–548. doi:10.1016/j.electacta.2019.01.040

Wu, N., Shen, J., Sun, L., Yuan, M., Shao, Y., Ma, J., et al. (2019b). Hierarchical N-Doped Graphene Coated 1D Cobalt Oxide Microrods for Robust and Fast Lithium Storage at Elevated Temperature. *Electrochimica Acta* 310, 70–77. doi:10.1016/j.electacta.2019.04.115

Xie, F., Zhang, L., Gu, Q., Chao, D., Jaroniec, M., and Qiao, S.-Z. (2019a). Multi-shell Hollow Structured Sb2S3 for Sodium-Ion Batteries with Enhanced Energy Density. *Nano Energy* 60, 591–599. doi:10.1016/j.nanoen.2019.04.008

Xie, J., Liu, L., Xia, J., Zhang, Y., Li, M., Ouyang, Y., et al. (2018). Template-Free Synthesis of Sb2S3 Hollow Microspheres as Anode Materials for Lithium-Ion and Sodium-Ion Batteries. *Nano-micro Lett.* 10 (1), 1–12. doi:10.1007/s40820-017-0165-1

Xie, J., Xia, J., Yuan, Y., Liu, L., Zhang, Y., Nie, S., et al. (2019b). Sb2S3 Embedded in Carbon-Silicon Oxide Nanofibers as High-Performance Anode Materials for Lithium-Ion and Sodium-Ion Batteries. *J. Power Sourc.* 435, 226762. doi:10.1016/j.jpowsour.2019.226762

Xing, Z., Tan, G., Yuan, Y., Wang, B., Ma, L., Xie, J., et al. (2020). Consolidating Lithiothermic-Ready Transition Metals for Li 2 S-Based Cathodes. *Adv. Mater.* 32 (31), 2002403. doi:10.1002/adma.202002403

Xiong, H., Slater, M. D., Balasubramanian, M., Johnson, C. S., and Rajh, T. (2011). Amorphous TiO2 Nanotube Anode for Rechargeable Sodium Ion Batteries. *J. Phys. Chem. Lett.* 2 (20), 2560–2565. doi:10.1021/jz2012066

Xiong, X., Wang, G., Lin, Y., Wang, Y., Ou, X., Zheng, F., et al. (2016). Enhancing Sodium Ion Battery Performance by Strongly Binding Nanostructured Sb2S3 on Sulfur-Doped Graphene Sheets. *ACS Nano* 10 (12), 10953–10959. doi:10.1021/acsnano.6b05653

Xu, B., Qi, S., He, P., and Ma, J. (2019). Antimony- and Bismuth-Based Chalcogenides for Sodium-Ion Batteries. *Chem. Asian J.* 14 (17), 2925–2937. doi:10.1002/asia.201900784

Yao, S., Cui, J., Deng, Y., Chong, W. G., Wu, J., Ihsan-Ul-Haq, M., et al. (2019). Ultrathin Sb2S3 Nanosheet Anodes for Exceptional Pseudocapacitive Contribution to Multi-Battery Charge Storage. *Energ. Storage Mater.* 20, 36–45. doi:10.1016/j.ensm.2018.11.005

Yin, W., Chai, W., Wang, K., Ye, W., Rui, Y., and Tang, B. (2019). A Highly Meso@Microporous Carbon-Supported Antimony Sulfide Nanoparticles Coated by Conductive Polymer for High-Performance Lithium and Sodium Ion Batteries. *Electrochimica Acta* 321, 134699. doi:10.1016/j.electacta.2019.134699

Yu, D. Y. W., Prikhodchenko, P. V., Mason, C. W., Batabyal, S. K., Gun, J., Sladkevich, S., et al. (2013). High-capacity Antimony Sulphide Nanoparticle-Decorated Graphene Composite as Anode for Sodium-Ion Batteries. *Nat. Commun.* 4, 1–7. doi:10.1038/ncomms3922

Yu, M., Yin, Z., Yan, G., Wang, Z., Guo, H., Li, G., et al. (2020). Synergy of Interlayer Expansion and Capacitive Contribution Promoting Sodium Ion Storage in S, N-Doped Mesoporous Carbon Nanofiber. *J. Power Sourc.* 449, 227514. doi:10.1016/j.jpowsour.2019.227514

Yu, S., Liu, Z., Tempel, H., Kungl, H., and Eichel, R.-A. (2018). Self-standing NASICON-type Electrodes with High Mass Loading for Fast-Cycling All-Phosphate Sodium-Ion Batteries. *J. Mater. Chem. A.* 6 (37), 18304–18317. doi:10.1039/c8ta07313a

Yuan, M., Guo, X., Liu, Y., and Pang, H. (2019). Si-based Materials Derived from Biomass: Synthesis and Applications in Electrochemical Energy Storage. *J. Mater. Chem. A.* 7 (39), 22123–22147. doi:10.1039/c9ta06934h

Zhai, H., Jiang, H., Qian, Y., Cai, X., Liu, H., Qiu, Y., et al. (2020). Sb2S3 Nanocrystals Embedded in Multichannel N-Doped Carbon Nanofiber for Ultralong Cycle Life Sodium-Ion Batteries. *Mater. Chem. Phys.* 240, 122139. doi:10.1016/j.matchemphys.2019.122139

Zhan, W., Zhu, M., Lan, J., Wang, H., Yuan, H., Yang, X., et al. (2021). 1D Sb2S3@nitrogen-Doped Carbon Coaxial Nanotubes Uniformly Encapsulated within 3D Porous Graphene Aerogel for Fast and Stable Sodium Storage. *Chem. Eng. J.* 408, 128007–128010. doi:10.1016/j.cej.2020.128007

Zhang, H., Ren, M., Jiang, W., Yao, J., Pan, L., and Yang, J. (2021a). Hierarchical Sb2S3@m-Ti3C2Tx Composite Anode with Enhanced Na-Ion Storage Properties. *J. Alloys Comp.* 887, 161318. doi:10.1016/j.jallcom.2021.161318

Zhang, Q., Zeng, Y., Wang, X., Wang, L., Wang, H., Xiao, J., et al. (2021b). Sb2S3 Nanoparticles Anchored on N-Doped 3D Carbon Nanofibers as Anode Material for Sodium Ion Batteries with Improved Electrochemical Performance. *J. Alloys Comp.* 881, 160594–160599. doi:10.1016/j.jallcom.2021.160594

Zhang, Z., Zhao, J., Xu, M., Wang, H., Gong, Y., and Xu, J. (2018). Facile Synthesis of Sb2S3/MoS2 Heterostructure as Anode Material for Sodium-Ion Batteries. *Nanotechnology* 29 (33), 335401. doi:10.1088/1361-6528/aac645

Zhao, W., Li, M., Qi, Y., Tao, Y., Shi, Z., Liu, Y., et al. (2021). Ultrasound Sonochemical Synthesis of Amorphous Sb2S3-Graphene Composites for Sodium-Ion Batteries. *J. Colloid Interf. Sci.* 586, 404–411. doi:10.1016/j.jcis.2020.10.104

Zhao, W., Zhang, L., Jiang, F., Chang, X., Yang, Y., Ge, P., et al. (2020). Engineering Metal Sulfides with Hierarchical Interfaces for Advanced Sodium-Ion Storage Systems. *J. Mater. Chem. A.* 8 (10), 5284–5297. doi:10.1039/c9ta13899d

Zhao, Y., and Manthiram, A. (2015). Amorphous Sb2S3 Embedded in Graphite: a High-Rate, Long-Life Anode Material for Sodium-Ion Batteries. *Chem. Commun.* 51 (67), 13205–13208. doi:10.1039/x0xx00000x10.1039/c5cc03825a

Zhao, Y., and Manthiram, A. (2015). Bi0.94Sb1.06S3 Nanorod Cluster Anodes for Sodium-Ion Batteries: Enhanced Reversibility by the Synergistic Effect of the Bi2S3-Sb2S3 Solid Solution. *Chem. Mater.* 27 (17), 6139–6145. doi:10.1021/acs.chemmater.5b02833

Zheng, T., Li, G., Zhao, L., and Shen, Y. (2018). Flowerlike Sb 2 S 3 /PPy Microspheres Used as Anode Material for High-Performance Sodium-Ion Batteries. *Eur. J. Inorg. Chem.* 2018 (10), 1224–1228. doi:10.1002/ejic.201701364

Zhou, J., Dou, Q., Zhang, L., Wang, Y., Yuan, H., Chen, J., et al. (2020a). A Novel and Fast Method to Prepare a Cu-Supported α-Sb2S3@CuSbS2 Binder-free Electrode for Sodium-Ion Batteries. *RSC Adv.* 10 (49), 29567–29574. doi:10.1039/d0ra05623e

Zhou, X., Zhang, Z., Yan, P., Jiang, Y., Wang, H., and Tang, Y. (2020b). Sulfur-doped Reduced Graphene oxide/Sb2S3 Composite for superior Lithium and Sodium Storage. *Mater. Chem. Phys.* 244, 122661–122668. doi:10.1016/j.matchemphys.2020.122661

Zhu, Y., Nie, P., Shen, L., Dong, S., Sheng, Q., Li, H., et al. (2015). High Rate Capability and superior Cycle Stability of a Flower-like Sb2S3anode for High-Capacity Sodium Ion Batteries. *Nanoscale* 7 (7), 3309–3315. doi:10.1039/c4nr05242k

Conflict of Interest: Author ZC was employed by the company Luoyang Bearing Research Institute Co., Ltd.

The remaining authors declare that the research was conducted in the absence of any commercial or financial relationships that could be construed as a potential conflict of interest

Publisher's Note: All claims expressed in this article are solely those of the authors and do not necessarily represent those of their affiliated organizations, or those of the publisher, the editors, and the reviewers. Any product that may be evaluated in this article, or claim that may be made by its manufacturer, is not guaranteed or endorsed by the publisher.